PNAS RESEARCH ARTICLE | CELL BIOLOGY

Multifaceted role for p53 in pancreatic cancer suppression

Stephano S. Mello[a,b], Brittany M. Flowers[a], Pawel K. Mazur[c], James J. Lee[d,e], Fabian Müller[f,g], Sarah K. Denny[f], Sofia Ferreira[a], Kathryn Hanson[a,f], Seung K. Kim[d], William J. Greenleaf[f], Laura D. Wood[h], and Laura D. Attardi[a,f,1]

Edited by Carol Prives, Columbia University, New York, NY; received July 14, 2022; accepted January 5, 2023

The vast majority of human pancreatic ductal adenocarcinomas (PDACs) harbor *TP53* mutations, underscoring p53's critical role in PDAC suppression. PDAC can arise when pancreatic acinar cells undergo acinar-to-ductal metaplasia (ADM), giving rise to premalignant pancreatic intraepithelial neoplasias (PanINs), which finally progress to PDAC. The occurrence of *TP53* mutations in late-stage PanINs has led to the idea that p53 acts to suppress malignant transformation of PanINs to PDAC. However, the cellular basis for p53 action during PDAC development has not been explored in detail. Here, we leverage a hyperactive p53 variant—p53^{53,54}—which we previously showed is a more robust PDAC suppressor than wild-type p53, to elucidate how p53 acts at the cellular level to dampen PDAC development. Using both inflammation-induced and KRAS^{G12D}-driven PDAC models, we find that p53^{53,54} both limits ADM accumulation and suppresses PanIN cell proliferation and does so more effectively than wild-type p53. Moreover, p53^{53,54} suppresses KRAS signaling in PanINs and limits effects on the extracellular matrix (ECM) remodeling. While p53^{53,54} has highlighted these functions, we find that pancreata in wild-type p53 mice similarly show less ADM, as well as reduced PanIN cell proliferation, KRAS signaling, and ECM remodeling relative to *Trp53*-null mice. We find further that p53 enhances chromatin accessibility at sites controlled by acinar cell identity transcription factors. These findings reveal that p53 acts at multiple stages to suppress PDAC, both by limiting metaplastic transformation of acini and by dampening KRAS signaling in PanINs, thus providing key new understanding of p53 function in PDAC.

p53 | pancreatitis | pancreatic cancer | ADM | PanIN

Significance

Despite being the most commonly mutated tumor suppressor gene in all cancers, and being highly mutated (75%) in pancreatic cancers, there are no standard-of-care therapies based on p53 used in the clinic. Understanding the cellular and molecular basis of p53 action is critical for developing such therapies. Here, we employ a mouse model expressing a mildly hyperactive p53 mutant protein to identify two new mechanisms through which p53 suppresses pancreatic cancer initiation: by opposing acinar cell metaplastic transformation and by dampening KRAS signaling in preneoplastic lesions. Our data support the idea that mild p53 activation could be used as a preventative therapy in patients at risk of developing pancreatic cancer.

Pancreatic ductal adenocarcinoma (PDAC) is a deadly disease with a dismal 5-y survival rate of just 10% (1). This poor prognosis relates both to the disease progressing to a very advanced stage without overt symptoms and to largely ineffective treatments. A better understanding of how to manage this disease would come from a clearer understanding of the molecular underpinnings of PDAC development. Understanding the molecular processes associated with tumor initiation and progression is paramount for the development of early detection markers and novel treatment strategies.

The analysis of human PDAC development through genetic and histological analyses has led to a model of disease pathogenesis (2, 3). Human cancer genome sequencing has shown that activating mutations in the *KRAS* oncogene are found in ~94% of human PDACs, suggesting that these mutations drive PDAC initiation (4). Histological studies suggested originally that PDAC initiates from pancreatic ductal cells, which develop into pre-malignant ductal-like precursor lesions known as pancreatic intraepithelial neoplasias (PanINs) and progress through increasingly more dysplastic stages known as PanIN1A, 1B, 2, and 3, resulting ultimately in invasive PDACs (5, 6). Subsequent lineage tracing experiments using mouse models showed, however, that despite their resemblance to pancreatic ducts, PanINs can be generated by a metaplastic event known as acinar-to-ductal metaplasia (ADM), whereby acinar cells undergo a dedifferentiation process, losing acinar characteristics and acquiring ductal characteristics (7–9). Indeed, oncogenic *Kras* expression in mouse acinar cells is sufficient to promote ADM, PanIN, and PDAC formation (10–14). Moreover, the detection of oncogenic *KRAS* mutations in human acinar cells and early PanIN1 lesions supports the notion that *KRAS* mutations also drive ADM, PanINs, and PDAC development in humans (13, 15, 16).

After *KRAS,* mutations in the *TP53, CDKN2A,* and *SMAD4* tumor suppressor genes (TSGs) are the most prevalent in human PDAC, with estimated mutation frequencies of 72, 30, and 32%, respectively (17). Mutations in these TSGs have been suggested to occur subsequent to *KRAS* mutations, during the progression of lower-grade PanINs to higher-grade PanINs or PDAC (18). Specifically, mutations in *CDKN2A* have been found in PanIN2 lesions and mutations in *TP53* and *SMAD4* have been detected in PanIN3 lesions, leading to the idea that these mutations are essential for the progression toward higher-grade lesions and ultimately PDAC. Notably, the progression from PanIN3 to metastatic

Author contributions: S.S.M. and L.D.A. designed research; S.S.M., B.M.F., P.K.M., S.F., S.K.D. and K.H. performed research; J.J.L., F.M., S.K.D., S.K., and W.J.G. contributed new reagents/analytic tools; S.M., P.M., L.D.A. and L.D.W. analyzed data; and S.M. and L.D.A. wrote the paper.

The authors declare no competing interest.

This article is a PNAS Direct Submission.

[1]To whom correspondence may be addressed. Email: attardi@stanford.edu.

This article contains supporting information online at https://www.pnas.org/lookup/suppl/doi:10.1073/pnas.2211937120/-/DCSupplemental.

Published February 27, 2023.

PDAC is frequently connected with loss of heterozygosity (LOH) of *TP53*, suggesting that p53 functions as roadblock to metastatic disease (19), consistent with mouse models studies showing that *Trp53* inactivation allows malignant progression (20). However, the conclusions about how these TSGs might restrain PDAC development are based on a limited number of studies, and some mutational analyses of early neoplastic lesions do not support this model, as they showed that *TP53* mutations can occur earlier in this process, in ADMs or in early PanINs (19, 21–24). Moreover, *TP53* mutations in PanIN3 were largely inferred by immunostaining for p53 protein (25), but this provides only an indirect assessment of *TP53* status, as positivity can reflect either accumulation of mutant p53 or stabilization of wild-type p53 in response to a stress signal. A more detailed investigation into the roles of these tumor suppressors in PDAC is therefore warranted. In particular, understanding how p53 acts, given its mutation in nearly 75% of PDACs, will provide great insight into PDAC development.

Despite being the most commonly-mutated gene in human cancer, the mechanisms by which p53 impedes tumor development remain incompletely understood. p53 is a transcriptional activator known to limit cell cycle progression or induce apoptosis in response to acute DNA damage, and it does so by transcriptionally activating target genes harboring p53 consensus binding sites, such as those encoding the CDK inhibitor p21 and the pro-apoptotic BCL2 family members NOXA and PUMA (26). While this capacity was envisioned originally to account for p53 tumor suppressor activity, studies in mouse models have shown that robust p53-mediated activation of these genes is dispensable for tumor suppression and that p53 regulates a variety of other cellular responses that might play a role in tumor suppression (26–31). Genetically engineered mouse models provide an opportunity to understand p53 action in an in vivo context, and will help to decipher how p53 inactivation promotes cancer development.

Here, we leverage mouse pancreatitis and oncogenic KRAS-driven PDAC models to dissect the cellular basis of p53 action in PDAC suppression. Specifically, we utilize p53 transcriptional activation domain (TAD) mutant mice that we generated previously. p53 harbors two distinct TADs, and our previous studies of knock-in mice expressing the TAD2 mutant, known as $p53^{53,54}$, demonstrated that this mutant act as a "super-tumor suppressor," suppressing PDAC better than wild-type p53. This $p53^{53,54}$ mutant characterized by enhanced tumor suppressor activity, which is at least in part attributable to hyperactivation of a small subset of p53 target genes (28), provides a useful tool to better understand the cellular mechanisms underlying p53-mediated tumor suppression in PDAC. Analyses with this mutant, then with wild-type p53, reveal multifaceted cellular effects of p53 during PDAC evolution, providing key new insight into how p53 suppresses pancreatic cancer development.

Results

Analysis of $p53^{53,54}$ Reveals a Role for p53 in Restraining ADM. Our previous findings revealed that the $p53^{F53Q,\ F54S}$ mutant (henceforth referred to as $p53^{53,54}$) displays enhanced pancreatic cancer suppressor activity relative to wild-type p53 (Fig. 1*A*). We reasoned that analysis of this mutant would provide a powerful strategy to better understand how p53 acts at the cellular level to dampen pancreatic cancer development. To understand the mechanisms of $p53^{53,54}$ action in restraining pancreatic cancer development, we used an established mouse PDAC model in which Cre expression under the control of the *Ptf1a* promoter drives the expression of oncogenic $KRAS^{G12D}$ in the embryonic pancreas (6). We then analyzed the early steps of PDAC development by subjecting mice to treatment with caerulein, an oligopeptide that stimulates secretion of digestive enzymes and causes acute pancreatitis, thereby enhancing ADM and PanIN formation (14). We generated $Kras^{LSL\text{-}G12D/+}$;$Ptf1a^{Cre/+}$ (*KC*) mice homozygous for either wild-type *Trp53* ($Trp53^{+/+}$) or $Trp53^{53,54}$ and treated them with caerulein (Fig. 1*B*). We then investigated how the $p53^{53,54}$ mutant affects the development of premalignant lesions by quantifying ADM and PanIN lesions.

We first examined the effect of $p53^{53,54}$ expression on ADM levels by evaluating pancreas sections from cohorts 1 wk after caerulein treatment by H&E staining and immunofluorescence analyses for specific acinar cell (AMYLASE) and ductal markers (CK19) (Fig. 1*C*). Interestingly, these analyses showed that mice homozygous for the $Trp53^{53,54}$ allele showed enhanced acinar preservation relative to wild-type *Trp53* mice, measured both by acinar area and the number of pancreatic lobes affected with ADM (Fig. 1*D*), suggesting that $p53^{53,54}$ restrains ADM. Of note, caerulein treatment induced similar levels of initial pancreatic damage in both cohorts, as determined by histological analysis 24 h after caerulein administration, suggesting that $p53^{53,54}$ is not preventing the initial damage, but rather promoting recovery from caerulein-induced damage (*SI Appendix*, Fig. S1*A*). To evaluate whether the effect of the $p53^{53,54}$ mutant on ADM is associated with enhanced cell division and faster regeneration, we analyzed KI67 positivity in ADMs and found that the reduced ADM observed in the $KC;Trp53^{53,54/53,54}$ mice was not accounted for by increased acinar cellular proliferation within ADM lesions after caerulein treatment (*SI Appendix*, Fig. S1*B*). Consistent with our previous observations that $p53^{53,54}$ protein is more stable than wild-type p53 (28), we found that ADMs from $KC;Trp53^{53,54/53,54}$ mice displayed higher p53 protein expression than those in $KC;Trp53^{+/+}$ mice (Fig. 1*E*). These findings suggest that the enhanced tumor suppressor activity of the $p53^{53,54}$ protein could relate at least in part to its ability to restrict ADM accumulation.

To independently confirm the enhanced capacity of $p53^{53,54}$ to restrain ADM, we also performed in vitro organoid cultures. In this assay, we used TGFα/EGF to induce ADM, as previously described (32), and we tested whether $p53^{53,54}$ can inhibit ADM in vitro, without the interference of other factors present in vivo, such as inflammation and the presence of stromal cells. Acini from $p53^{+/+}$ and $p53^{53,54/53,54}$ mice were isolated and resuspended in collagen, in the presence of TGFα/EGF, and the extent of ADM was assayed 5 d later. The results confirmed what was seen in vivo, with $p53^{53,54}$ acini showing a greater resistance to ADM than wild-type *Trp53* counterparts in a stroma-free environment (Fig. 1 *F* and *G*). These findings underscore the cell autonomous mode of action for $p53^{53,54}$ in suppressing ADM. Together, these findings describe a novel role of p53 in restraining initial transformation steps in the pancreas.

$p53^{53,54}$ Inhibits PanIN Proliferation after Pancreatitis. Despite the strong capacity of $p53^{53,54}$ to preserve acinar structure, we did observe the formation of some PanINs in the pancreata of caerulein-treated $KC;Trp53^{53,54/53,54}$ mice, raising the possibility that $p53^{53,54}$ might act through additional mechanisms in PanINs. Given that p53 is found to be mutated in late PanINs in humans, we examined whether $p53^{53,54}$ might also suppress PDAC development through effects on PanIN expansion. To this end, we evaluated features of PanINs in the caerulein-treated cohort described above. We identified PanIN lesions by H&E staining and staining for Alcian Blue and MUC5AC, well-established markers of PanINs (6). First, by quantifying the number of

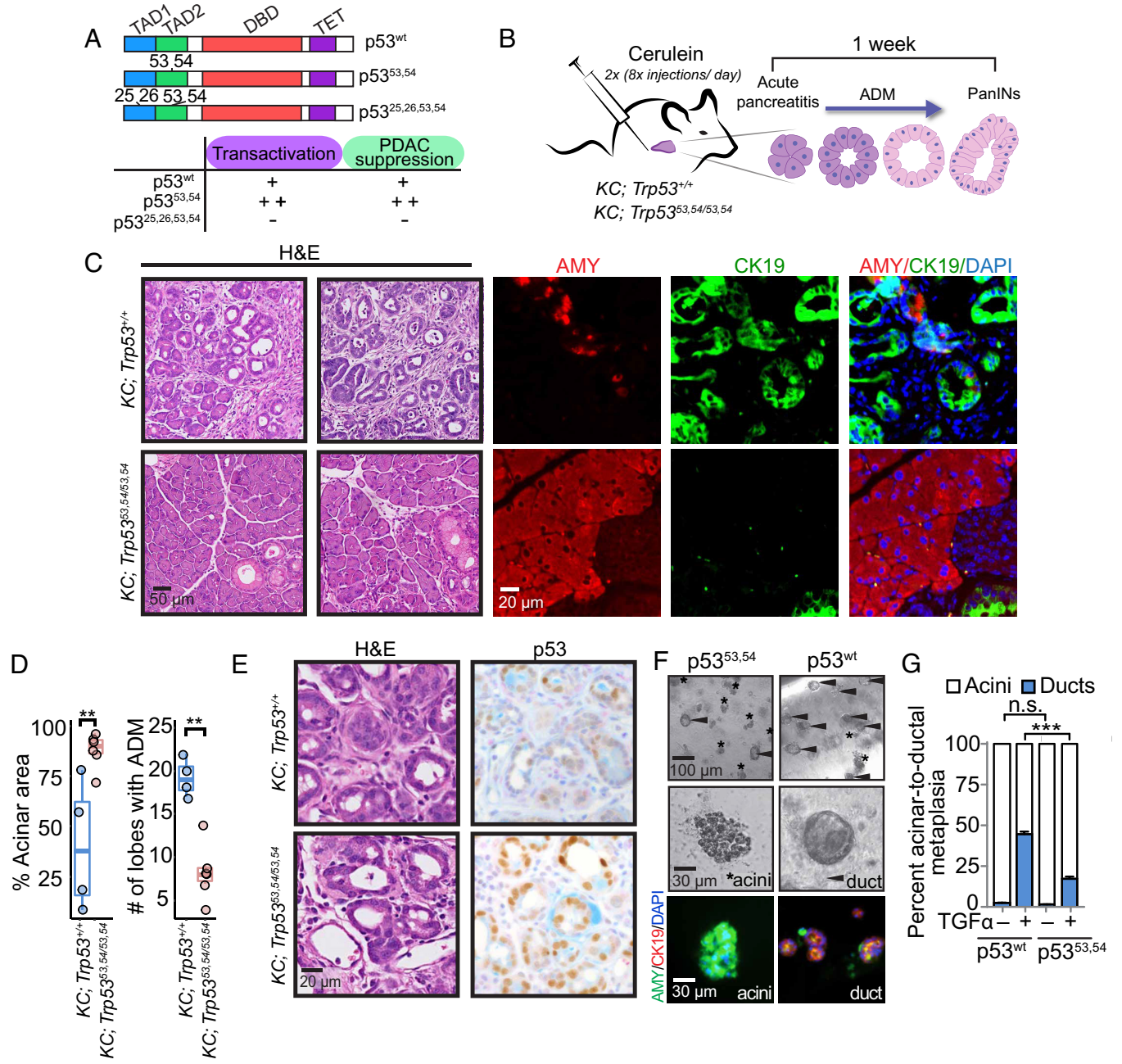

Fig. 1. p53^{53,54} restrains ADM in caerulein-treated mice. (*A*) Schematic representation of wild-type and TAD mutant p53 proteins (TAD—transcriptional activation domain, DBD–DNA binding domain, TET—tetramerization domain) and a summary of their respective transactivation and PDAC suppression activities. p53^{53,54} is able to hyperactivate a subset of p53 target genes. (*B*) Schematic of caerulein-induced acute pancreatitis and its sequelae within 1 wk after treatment, including ADM and formation of PanINs. (*C*) Representative histological images of lesions found in caerulein-treated 2-mo-old *KC;Trp53*$^{+/+}$ and *KC;Trp53*$^{53,54/53,54}$ mice 1 wk after caerulein-induced acute pancreatitis. Two H&E fields and a higher magnification field immunostained for AMYLASE (AMY), CYTOKERATIN 19 (CK19) and DAPI are shown for each genotype. (*D*) Quantification of pancreatic transdifferentiation in entire pancreas using two different parameters: (*Left*) The percentage of acinar area relative to the whole pancreas ± SD based on H&E staining and (*Right*) the number of pancreatic lobes with ADM ± SD based on H&E staining (n = 4 for *KC;Trp53*$^{+/+}$ cohort and n = 6 for *KC;Trp53*$^{53,54/53,54}$ cohort. (*E*) Representative p53 immunostaining in ADM in *KC;Trp53*$^{+/+}$ and *KC;Trp53*$^{53,54/53,54}$ mice. (*F*) Ex vivo ADM assay in TGFα-treated acini from *Trp53*$^{+/+}$ and *Trp53*$^{53,54/53,54}$ mice. (*Top*) Representative brightfield images of acinar cultures showing the presence of ductal-like spheroid structures (arrowheads) in the midst of acinar cells (asterisks). (*Middle*) High magnification view of ductal and acinar structures using brightfield microscopy and (*Bottom*) High-magnification view of ductal and acinar structures immunostained for AMY, CK19 and DAPI (*G*) Average percentage of ADM ± SEM in independent biological replicates (n = 4 for both *Trp53*$^{+/+}$ and *Trp53*$^{53,54/53,54}$ cohorts), measured based on the morphological appearance of seeded acini. Normal acini show a grape-like clustered shape, while metaplastic acini undergoing ADM acquire a bubble-like shape. ** and *** represent $P \leq 0.01$ and 0.001, respectively, based on the two-tailed unpaired Student's *t* test. Blue and pink circles represent individual *KC;Trp53*$^{+/+}$ and *KC;Trp53*$^{53,54/53,54}$ mice respectively.

MUC5AC-positive cells in the pancreata of each cohort, we found that *KC;Trp53*$^{53,54/53,54}$ mice showed decreased PanIN formation relative to *KC;Trp53*$^{+/+}$ mice, suggesting that the ability of this mutant to restrain ADM contributes to decreased PanIN formation (Fig. 2 *A* and *B*). Second, PanINs in *KC;Trp53*$^{53,54/53,54}$ mice displayed decreased proliferation, based on KI67 positivity, and increased levels of senescence, as assessed by SA-β-galactosidase positivity, compared to those in *KC;Trp53*$^{+/+}$ mice (Fig. 2 *A*, *C*, and *D*). Notably, p53 was detectable by immunohistochemistry in some PanINs in *KC;Trp53*$^{53,54/53,54}$ mice but not in *KC;Trp53*$^{+/+}$ mice, providing a potential explanation for its enhanced potency (Fig. 2*E*). Thus, beyond the effects of p53^{53,54} on ADM, these

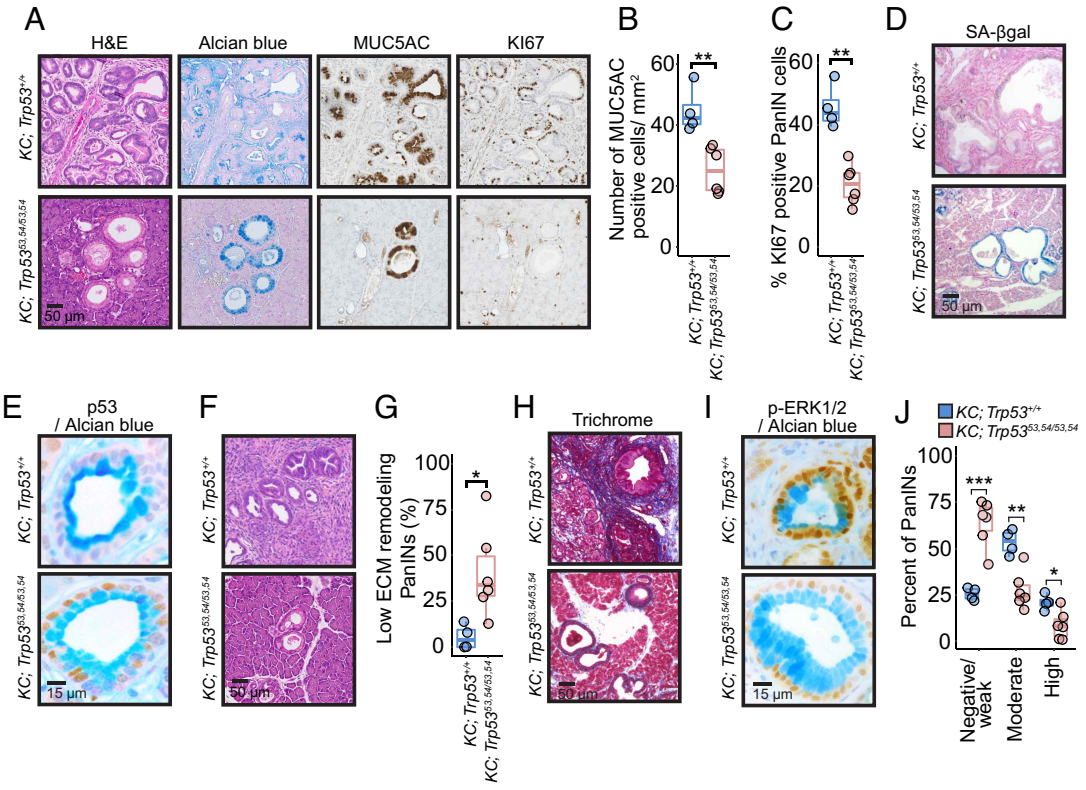

Fig. 2. p53^{53,54} Restrains PanIN Progression in Caerulein-Treated Mice. (*A*) Representative histological images of PanINs found in caerulein-treated *KC;Trp53*$^{+/+}$ and *KC;Trp53*$^{53,54/53,54}$ mice 1 wk after caerulein treatment. H&E, Alcian Blue, MUC5AC, and KI67 staining are shown. (*B*) The number of MUC5AC positive cells per square millimeter in pancreata (n = 4 for *KC;Trp53*$^{+/+}$ cohort and n = 6 for *KC;Trp53*$^{53,54/53,54}$ cohort, a total of 25 fields per mouse were counted). (*C*) The percentage of Alcian Blue-positive PanIN cells that were KI67 positive in pancreata of each cohort (n = 4 for *KC;Trp53*$^{+/+}$ cohort and n = 6 for *KC;Trp53*$^{53,54/53,54}$ cohort, a total of 25 fields per mouse were counted). (*D*) Representative SA-βgalactosidase staining in pancreata. (*E*) Representative p53 immunostaining in PanINs, as identified by Alcian Blue staining (*F*) Representative H&E images showing PanINs and surrounding ECM remodeling. (*G*) The percentage of PanINs in entire pancreas, based on MUC5AC staining, that show low ECM remodeling, defined by H&E analysis, ± SD from (n = 4 and 6 for *KC;Trp53*$^{+/+}$ and *KC;Trp53*$^{53,54/53,54}$ mice, respectively). (*H*) Masson's Trichrome staining in pancreata of mice from both cohorts. (*I*) Representative images of PanINs, marked by Alcian Blue staining, showing phospho-ERK1/2 staining. (*J*) The percentage of PanINs in entire pancreas with negative/weak, moderate or high levels of phospho-ERK1/2 ± SD (n = 4 and six mice for *KC; Trp53*$^{+/+}$ and *KC; Trp53*$^{53,54/53,54}$ mice, respectively), based on phospho-ERK1/2/Alcian Blue immunostaining. Data represent mean ± SD; *, ** and *** represent $P \leq 0.05$, 0.01 and 0.001, respectively, based on the two-tailed unpaired Student's *t* test. Blue and pink circles represent individual *KC;Trp53*$^{+/+}$ and *KC;Trp53*$^{53,54/53,54}$ mice, respectively.

findings suggest together that p53^{53,54} also inhibits disease progression by inhibiting cell division in PanINs and inducing senescence.

Interestingly, H&E staining also revealed that the PanINs in *KC;Trp53*$^{53,54/53,54}$ mice were remarkably different histologically from those found in caerulein-treated *KC;Trp53*$^{+/+}$mice. PanINs can be accompanied by extracellular matrix (ECM) remodeling (33, 34). In the *KC;Trp53*$^{53,54/53,54}$ mice, we noted a strongly diminished ECM remodeling around the observed PanIN lesions, which were instead surrounded by normal acinar parenchyma, unlike those in *KC;Trp53*$^{+/+}$ mice (Fig. 2 *A, F*, and *G*). This observation was supported by Trichrome staining, which showed reduced collagen deposition in pancreata of *KC;Trp53*$^{53,54/53,54}$ mice relative to pancreata in *KC;Trp53*$^{+/+}$ mice (Fig. 2*H*). Since the pancreatic desmoplastic reaction has been associated with persistent KRAS signaling (34), we examined whether p53^{53,54} expression is associated with reduced KRAS activity in PanINs. We performed immunostaining for the KRAS signaling marker phospho-ERK1/2 and quantified ERK activation in PanINs marked by Alcian Blue in *KC;Trp53*$^{+/+}$and *KC;Trp53*$^{53,54/53,54}$ mice. We parsed PanIN lesions into three categories, binning them according to p-ERK1/2 staining intensity (*SI Appendix*, Fig. S2) and quantified the number of PanINs in each category in both cohorts. These results revealed that the p53^{53,54} mutant dampens ERK1/2 phosphorylation in precursor lesions, reflecting decreased KRAS activity (Fig. 2 *I* and *J*). Together, these findings suggest that the enhanced tumor suppressive ability of p53^{53,54} may be at least in part related to its capacity to constrain oncogenic KRAS signaling.

p53^{53,54} Inhibits ADM and PanIN Proliferation in a Kras^{G12D}-Driven PDAC Model. Although caerulein-induced acute pancreatitis is a reproducible way to accelerate PDAC in mouse models, we sought to address the effects of this hyperactive p53^{53,54} mutant in the development of *Kras*^{G12D}-driven PDAC in aging mice. To this end, we aged *KC;Trp53*$^{+/+}$ and *KC;Trp53*$^{53,54/53,54}$ mice for 5 mo, a time point when premalignant lesions but not cancer are typically observed (28). At the end of this period, we performed a histological evaluation of the pancreas to examine ADM and PanIN burden. As observed in caerulein-treated mice, normal acinar tissue structure was largely preserved in p53^{53,54} mice relative to mice with wild-type p53, as determined by H&E staining (Fig. 3 *A* and *B*). We also observed a decrease in PanIN burden, as assessed by Alcian Blue staining (Fig. 3*C*). PanINs that formed in *KC;Trp53*$^{53,54/53,54}$ mice were also less proliferative than those in *KC;Trp53*$^{+/+}$ mice (Fig. 3*D*). Trichrome staining showed further that there was much less stromal reaction in the pancreata of *KC;Trp53*$^{53,54/53,54}$ mice than in controls (Fig. 3*E*). Finally, we also observed reduced ERK1/2 phosphorylation in PanINs of *KC;Trp53*$^{53,54/53,54}$ mice relative to control counterparts, suggesting that the p53^{53,54} mutant can also

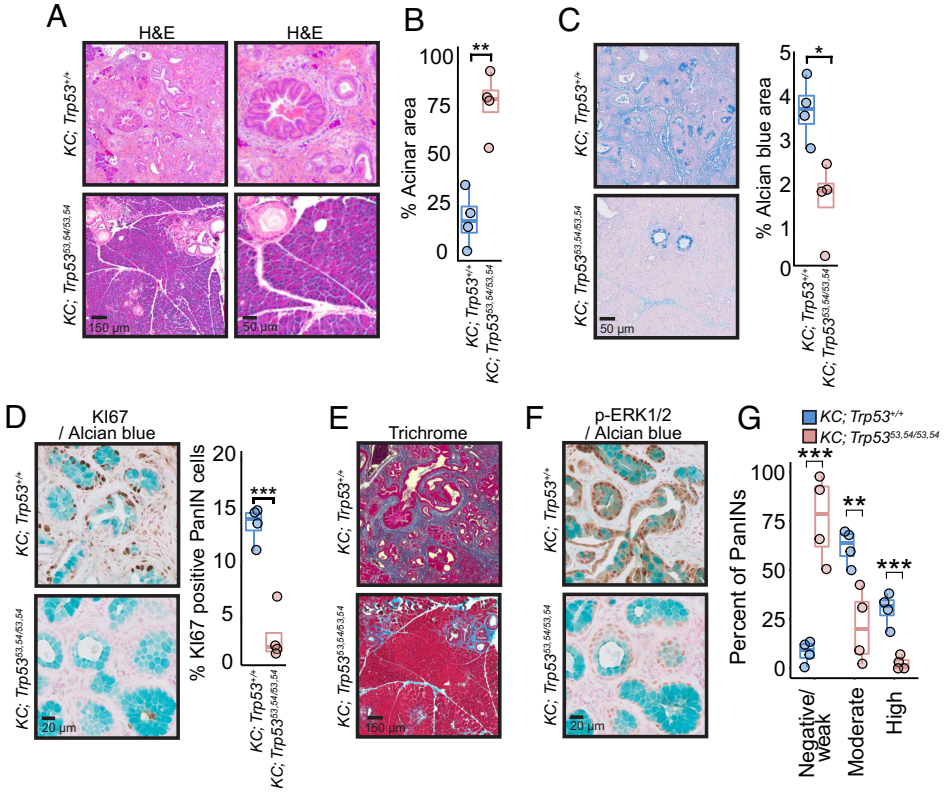

Fig. 3. p53^{53,54} Restrains Disease Progression in Aging *Kras* Mice. (*A*) Representative H&E images of 5-mo-old *KC;Trp53*$^{+/+}$ and *KC;Trp53*$^{53,54/53,54}$ mice. (*B*) The percentage of pancreas area comprising normal acini ± SD, based on H&E staining from n = 4 and 6 for *KC;Trp53*$^{+/+}$ and *KC;Trp53*$^{53,54/53,54}$ mice, respectively. Quantification was performed on the entire pancreas. (*C*) (*Left*) Representative Alcian Blue images and (*Right*) percentage of pancreas area comprising PanINs, based on Alcian Blue staining, ± SD for each cohort (n = 4 and 6 for *KC;Trp53*$^{+/+}$ and *KC;Trp53*$^{53,54/53,54}$ mice, respectively). Quantification was performed on the entire pancreas. (*D*) (*Left*) Representative Alcian Blue (to mark PanIN lesions) and KI67 immunostaining for each cohort is shown. (*Right*) Quantification of KI67-positive Alcian Blue-positive PanIN cells ± SD (n = 4 and 6 for *KC;Trp53*$^{+/+}$ and *KC;Trp53*$^{53,54/53,54}$ mice, respectively). A total of 25 fields per mouse were counted. (*E*) Representative Masson's Trichrome staining in pancreata of mice from each cohort. (*F*) Representative images of phospho-ERK1/2/Alcian Blue immunostaining for each cohort. (*G*) The percentage of PanINs with negative/weak, moderate or high levels of phospho-ERK1/2 ± SD from n = 4 and 6 for *KC;Trp53*$^{+/+}$ and *KC;Trp53*$^{53,54/53,54}$ mice, respectively. Quantification was performed on the entire pancreas. Data represents mean ± SD; *, ** and *** represent $P \le 0.05$, 0.01 and 0.001, respectively, based on the two-tailed unpaired Student's *t* test. Blue and pink circles represent individual *KC;Trp53*$^{+/+}$ and *KC;Trp53*$^{53,54/53,54}$ mice respectively.

limit KRAS signaling in conditions where pancreatitis is not involved (Fig. 3 *F* and *G*). Collectively, these findings show that the p53^{53,54} mutant limits ADM accumulation, PanIN proliferation, stromal reaction, and KRAS signaling in *Kras*^{G12D}-driven pancreatic cancer.

Wild-Type p53 Suppresses ADM and PanIN Proliferation in a Kras^{G12D}-Driven PDAC Model. Our studies of the stabilized p53^{53,54} mutant suggest that p53 is able to exert tumor suppressive effects both through blocking ADM and inhibiting PanIN progression. We next sought to interrogate whether wild-type p53 acts through similar mechanisms, by analyzing aging *Kras*^{G12D}-expressing mice prone to PDAC. We examined histology of pancreata in *KC;Trp53*$^{+/+}$and *KC;Trp53*$^{fl/fl}$ mice at 7 wk of age using H&E staining and immunofluorescence for markers of normal acinar cells (AMYLASE) and ductal-like lesions (CK19; Fig. 4 *A* and *B*). We observed that the *p53*-deficient mice exhibit profuse ADM and loss of acinar cells, while p53 wild-type mice retained normal acinar structure. We further observed that wild-type p53 is stabilized during ADM in aging *Kras*^{G12D}-expressing mouse pancreata, suggesting that wild-type p53 acts in ADMs to suppress preneoplastic stages of oncogenic KRAS-initiated pancreas tumorigenesis (Fig. 4*C*). Interestingly, we found that wild-type p53 promotes acinar cell regeneration after caerulein-induced injury in mice expressing wild-type *Kras*, indicating that the role of wild-type p53 in promoting acinar cell identity after injury is not restricted to a cancer context (*SI Appendix*, Fig. S3).

To further gauge the effect of loss of wild-type *Trp53* in PDAC development, we examined 7-wk-old *KC;Trp53*$^{+/+}$ and *KC;Trp53*$^{fl/fl}$ mice to evaluate the role of wild-type p53 in suppressing PanINs. Using H&E and Alcian Blue staining for PanIN identification and CK19 staining for the identification of any type of ductal-like lesions, we observed that *Trp53* loss led to an increase in PanIN formation, consistent with the increased ADM observed with *Trp53* deficiency, as well as an increase of CK19+ lesions (Fig. 4 *D* and *E*). Interestingly, we observed a decreased percentage of CK19+ lesions that were also Alcian Blue positive in *KC;Trp53*$^{fl/fl}$ mice than in *KC;Trp53*$^{+/+}$ mice, suggesting that p53 loss might alter the trajectory of KRAS-driven PanIN formation, driving a non-mucinous preneoplastic state (*SI Appendix*, Fig. S3 *A* and *B*). We also found that *Trp53* loss increased proliferation in PanINs, as demonstrated by KI67 staining (Fig. 4*F*). In addition, trichrome staining was enhanced in pancreata of the *Trp53*-deficient cohort, suggesting an augmented ECM remodeling/stromal response (Fig. 4*G*). These results suggest that wild-type p53 also inhibits disease progression by limiting PanIN proliferation and stromal reaction. Together, our findings support the notion that p53 plays a dual role in opposing early events in PDAC formation, by suppressing both ADM and PanIN expansion (Fig. 4*H*).

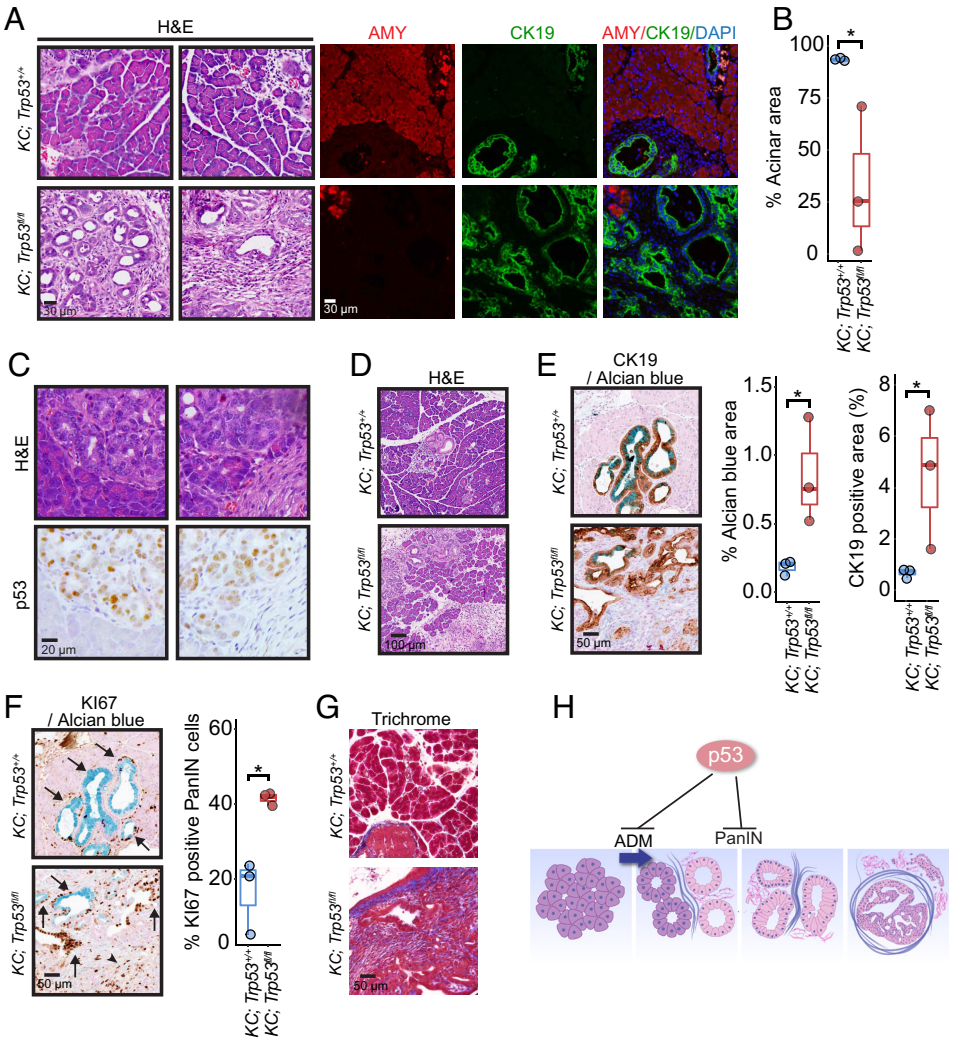

Fig. 4. Wild-Type p53 Restrains ADM and PanINs in Aging *Kras*^{G12D} Mice. (*A*) Representative histological images of lesions found in 7-wk-old *KC;Trp53*$^{+/+}$ and *KC;Trp53*$^{fl/fl}$ mice. H&E staining and immunostaining for AMYLASE (AMY), CYTOKERATIN 19 (CK19) and DAPI are shown for each genotype. (*B*) The percentage of pancreas area comprising normal acinar cells ± SD (n = 3 for both *KC;Trp53*$^{+/+}$ and *KC;Trp53*$^{fl/fl}$ mice). Quantification was performed on the entire pancreas, based on H&E staining. (*C*) Two representative H&E and p53 immunohistochemistry images of 7-wk-old *KC;Trp53*$^{+/+}$mice showing p53 positive cells in ADM areas. (*D*) Representative H&E images of PanINs found in 7-wk-old *KC;Trp53*$^{+/+}$ and *KC;Trp53*$^{fl/fl}$ mice. (*E*) (*Left*) Representative Alcian Blue (a marker of PanINs) and CK19 (a marker of normal ducts, PanINs and PDAC) staining, (*Right*) quantification of Alcian Blue and CK19 positive area ± SD from *KC;Trp53*$^{+/+}$ and *KC;Trp53*$^{fl/fl}$ mouse pancreata (n = 3 for both *KC;Trp53*$^{+/+}$ and *KC;Trp53*$^{fl/fl}$ mice). Quantification was performed on the entire pancreas. (*F*) (*Left*) Representative Alcian Blue and KI67 staining for each genotype and (*Right*) quantification of Alcian Blue-positive PanIN cells that are KI67 positive (arrows) ± SD (n = 3 for both *KC;Trp53*$^{+/+}$ and *KC;Trp53*$^{fl/fl}$ mice). Quantification was performed by counting positive cells in a total of 25 fields per mouse, as described in *Materials and Methods*. (*G*) Representative Masson's Trichrome stain in pancreata of each genotype. (*H*) Schematic of the different steps at which p53 can impede PDAC development. p53 can inhibit ADM and consequent PanIN formation, as well as PanIN cell proliferation. Data represent mean ± SD; * represents $P \leq 0.05$, based on the two-tailed unpaired Student's *t* test. Blue and red circles represent individual *KC;Trp53*$^{+/+}$ and *KC;Trp53*$^{fl/fl}$ mice, respectively.

p53 Promotes Chromatin Accessibility at Sites Controlled by Acinar Cell Identity Transcription Factors. To understand how p53 might promote the acinar cell state, we examined the chromatin landscape in acinar cells from *KC;Trp53*$^{+/+}$and *KC;Trp53*$^{fl/fl}$ mice. To this end, we sorted CD49F+, CD133- cells from pancreata of *KC;Trp53*$^{+/+}$and *KC;Trp53*$^{fl/fl}$ mice at ~3 and 1 mo of age respectively, stages characterized by similar levels of normal acinar cells in the two genotypes (Fig. 5*A* and *SI Appendix*, Fig. S4), then subjected them to ATAC-seq analysis (Fig. 5*B*). These studies revealed a set of regions more and less accessible with *Trp53* deletion (Fig. 5*C*). LOLA analysis of published pancreatic ChIP-seq data showed that regions open in the presence of p53 include known areas bound by the acinar cell identity factors PTF1A and RBPJL (Fig. 5*D*). Furthermore, motif analysis of the binding sites for transcription factors found in regions more accessible in the presence of p53 uncovered an enrichment for sites associated with PTF1A (E-BOX motif) and RBPJL. Indeed, genes that are more accessible in p53-expressing cells by ATAC-seq include hallmark RBPJL / PTF1A targets, such as *Cela1*, *Serpina6*, and *Klk10* (Fig. 5*E*). These observations suggest that in the presence of p53, regions associated with pancreatic identity factor binding become more accessible and suggest a mechanism by which p53 promotes acinar cell fate (Fig. 5*F*).

Discussion

Here, we directly interrogated the cellular mechanisms by which p53 impedes PDAC initiation and progression by leveraging a mildly hyperactive *p53* allele, encoding the p53^{53,54} TAD2 "super-tumor suppressor" mutant, which we showed previously has enhanced potential to suppress PDAC relative to wild-type p53 (28). We explored PDAC initiation and progression in oncogenic *Kras*-expressing mice using both acute pancreatitis and *Kras*^{G12D}-driven models. These studies revealed that relative to wild

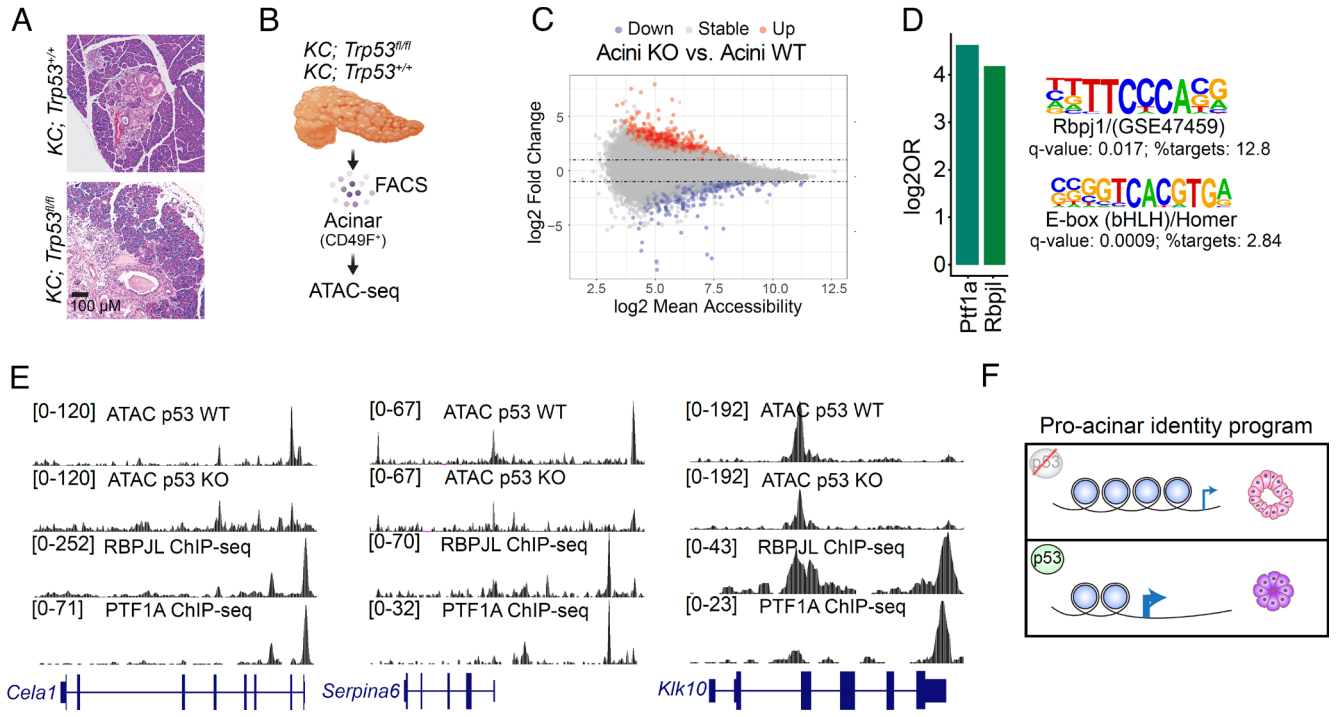

Fig. 5. p53 Promotes Chromatin Accessibility at Sites Controlled by Acinar Cell Identity Transcription Factors. (*A*) Representative H&E images of the pancreas of 3-mo-old and 1-mo-old *KC;Trp53*$^{+/+}$ and *KC;Trp53*$^{fl/fl}$ mice used for ATAC-seq experiments. (*B*) Schematic representation of the experimental steps for ATAC-seq experiments. (*C*) Scatter plot of log-twofold change differences between p53-proficient and p53-deficient acini, versus the Log2 mean accessibility. Red (enhanced accessibility) and blue (decreased accessibility) indicate significant accessibility changes. (*D*) (*Left*) LOLA analysis of regions that are more accessible in the presence of p53 using pancreas ChIP-seq data sets and (*Right*) Homer motif analysis of the factors found enriched by LOLA (*E*) Accessibility tracks from p53-proficient and deficient acini, for acinar genes controlled by RBPJL and PTF1A, as well as RBPJL and PTF1A ChIP-seq tracks. (*F*) Schematic of the role of p53 in promoting chromatin accessibility at pro-acinar identity genes.

type, the p53[53,54] mutant both more profoundly inhibits ADM accumulation, which reduces the formation of PanINs, and suppresses proliferation of PanIN cells, suggesting that p53 acts at multiple stages of PDAC development to impede disease. By comparing PDAC-prone aging mice carrying wild-type and *p53* conditional knockout alleles, we found further that wild-type p53 similarly inhibits both ADM accumulation and PanIN progression. Thus, rather than one specific mechanism for p53 action in tumor suppression at a particular stage of pancreatic cancer progression, these studies support a more complex function for p53 as a tumor suppressor at multiple points of disease development. This model contrasts with previous studies reporting that *TP53* mutations are mostly observed in advanced PanIN lesions, leading to the idea that p53-mediated tumor suppression occurs late in PDAC progression (18). Notably, a recent study using a PDAC mouse model in which *p53* LOH could be measured with a fluorescent reporter showed that *p53* LOH was observed in ADMs, supporting the importance of p53 tumor suppressive action in ADMs (35).

The use of pancreatitis models, in which caerulein synchronously induces ADM, has helped to uncover a role for p53 in restricting ADM, a reprogramming process that is associated with injury repair. Our panel of p53 variants—ranging from hyperactive to null—showed that the greater the p53 activity, the better the acinar character of the pancreas is maintained in oncogenic Kras-expressing mice, with fewer PanINs forming. Moreover, even in the backdrop of wild-type Kras, we observed that pancreata in mice expressing wild-type p53 regenerate to form normal acinar cells in response to caerulein treatment faster than those with p53 inactivation, suggesting that p53 helps to promote injury repair in a non-cancer context. The ability of p53 to promote acinar cell identity is consistent with our analysis of the chromatin landscape by ATAC-seq, where we observed that p53 promotes accessibility of sites associated with binding of the key acinar cell identity transcription factors, PTF1A and RBPJL. This role for p53 in restricting ADM accumulation is in keeping with the previously described ability of p53 to impede reprogramming of differentiated cells to iPS cells (36–38), as well as with studies showing that p53 restricts cellular plasticity and enforces cell fate when suppressing liver and pancreatic cancer (39, 40).

Our studies showed that p53 also restricts disease progression at the PanIN level. With increasing p53 activity, we observed reduced PanIN cell proliferation and cellular senescence, responses that can help limit progression of these lesions to malignant PDAC. This response reflects a more classical p53 function in dampening cell proliferation, and indeed, previous studies have suggested that the tumor suppressive capacity of p53 in pancreatic cancer lies in its ability to trigger senescence in PanIN lesions (41). We also observed that p53 limits preneoplastic lesion character to a more mucinous state. The idea that p53 exerts tumor suppressive effects in PanINs is consistent with the fact that LOH of *TP53* is a late event in PDAC progression, observed in advanced PanINs, and is thought to be essential for the progression from PanINs to PDAC (19). The idea that p53 plays a role only at later stages of PDAC development, however, became widespread, while the possibility that p53 could play a role in tumor suppression at earlier time points went unexplored. Importantly, reports suggest that *TP53* heterozygous mutations are also observed in early pancreatic lesions, such as in ADM and PanIN1A/1B stages, supporting our hypothesis that p53 function is also critical at earlier time points (19, 21, 23, 42). It is tempting to speculate that mutation of one *p53* allele could facilitate ADM and PanIN formation, while loss of the second *p53* allele is critical for progression of PanINs to PDAC.

We also observed that increased p53 activity and enhanced suppression of tumorigenesis is associated with dampened KRAS signaling in PanINs and inhibition of ECM remodeling. It is unclear whether p53 directly modulates KRAS signaling, thereby leading to suppression of ADM and disease progression, or whether KRAS is downregulated indirectly as a consequence of p53 changing cell state. Of note, dampened KRAS signaling in the presence of p53 has been observed in other contexts, such as in mouse lung adenocarcinoma models (43, 44). We also observed that in the presence of active p53, less collagen deposition is seen around lesions and normal acinar structure surrounds PanINs, consistent with reduced KRAS signaling.

A key question in this study is whether these new roles of p53 in PDAC suppression are cell autonomous or non-cell autonomous, since the $p53^{53,54}$ mouse model used in these experiments expresses this mutant protein in all tissues. A clear cell-intrinsic function is supported by our in vitro ADM organoid assays which showed that acini harboring the $p53^{53,54}$ allele have an enhanced acinar preservation capacity relative to wild-type *p53* acini in the absence of other cell types, such as stroma-associated fibroblasts or immune cells. Importantly, the conclusions we derived based on studying $p53^{53,54}$ mice were supported by experiments comparing *p53* wild-type and $p53^{fl}$ mice, where p53 status only differed in the acinar cells but not the stromal cells. Collectively, our findings suggest that these novel mechanisms of p53-mediated PDAC suppression are cell autonomous.

Our findings with the $p53^{53,54}$ mutant protein suggest that mild p53 activation could be used as a treatment strategy to limit pancreatic metaplasia and PDAC initiation. Notably, while showing enhanced tumor suppressor activity, $p53^{53,54}$ fails to trigger deleterious phenotypes typical of hyperactive p53 mutants (45–48). Therefore, as improved p53 activators are developed (49), it may be feasible to use mild p53 activation as a therapeutic strategy in patients at risk of developing PDAC, such as patients that suffer from chronic pancreatitis or with a familial history of PDAC. Future work exploring p53 activation as a preventative treatment for PDAC will be important for improved clinical management of patients at risk of developing PDAC.

Materials and Methods

Mouse Models. All animal experiments were performed according to Stanford University's APLAC (Administrative Panel on Laboratory Animal Care). $p53^{53,54}$ (27, 28) and $p53^{fl}$ mice (50) were bred to a mouse model for pancreatic cancer carrying $Kras^{LSL\text{-}G12D}$ (51) and a $Ptf1a^{Cre}$ allele (6) that induces the expression of mutant Kras specifically in the pancreas. For pancreatitis experiments, the mice were aged for 2 mo and treated with caerulein (100 μg per kilogram of body weight; Sigma-Aldrich) over 2 d, as previously described (52). For aging experiments, the mice were aged for either 5 mo or 7 wk, depending on the genotypes being studied.

Tissue Staining and Immunohistochemistry. Hematoxylin and eosin (H&E), Masson's Trichrome, Alcian Blue, and SA-βGal stainings were performed on tissue sections using standard protocols. Immunohistochemistry was performed using antibodies against CYTOKERATIN19 (TROMA-III; 1:200, DSHB-University of Iowa), AMYLASE (#3796; 1:3,000; Cell Signaling), p53 (CM-5; 1:500; Leica), MUC5AC (145-P1; 1:500, Thermo Scientific), KI67 (#550609; 1:100; BD Pharmingen), and phospho-ERK1/2 (#9101; 1:200; Cell Signaling). All the stains were performed using the VECTASTAIN Elite ABC HRP Kit (Vector Laboratories), according to the manufacturer's instructions. The sections were counterstained with hematoxylin or Alcian Blue/nuclear fast red. Immunofluorescence staining for CYTOKERATIN19 and AMYLASE was performed using anti-goat Alexa 488 (1:200; Invitrogen) and anti-rat Alexa 594 (1:200; Invitrogen) and counterstained with DAPI. Pictures were taken using a Leica microscope and/or with a NanoZoomer 2.0-RS slide scanner (Hamamatsu). The quantification of specific stains was performed in whole sections using ImageJ. In brief, the regions of interest (e.g., DAB stain, Alcian Blue) were selected based on its color and a binary image was created in ImageJ. Next, the "analyze particles" function was used to count and calculate the area of specific stain. For quantifications specified as "percent area," the area for the regions of interest was quantified as a ratio of the pancreas area. For quantifications of "percent of positive cells," 25 fields per mouse were used to count the cells of interest as "positive" or "negative" for a given marker, and the data used to calculate the percent of positive cells. The analysis of low stroma PanINs and phospho-ERK levels in PanINs was not performed using ImageJ, but rather manually counted in whole sections. Lobes with ADM were also counted manually, using a wide-field view of the slides.

In Vitro Organoid System and ADM Assays. Ex vivo ADM assays were performed using an organoid system. Acinar cultures from $p53^{+/+}$ and $p53^{53,54/53,54}$ mice (n = 4 for each cohort) were established from 4- to 8-wk–old $p53^{+/+}$ and $p53^{53,54/53,54}$ mice by modification of previously published protocols (53, 54). In brief, the whole pancreas was collected and treated twice with 1.2 mg mL collagenase VIII (Sigma-Aldrich). Following multiple wash steps with McCoy's medium containing soybean trypsin inhibitor (SBTI, 0.2 mg/mL), digested samples were filtered through a 100-μm filter, resuspended in culture medium (Waymouth's MB 752/1 supplemented with 0.1% BSA, 0.2 mg/mL SBTI; 50 μg/mL bovine pituitary extract, 10 μg/mL insulin, 5 μg/mL transferrin, 6.7 ng/mL selenium and 30% FCS) and allowed to recover for 1 h at 37 °C. Then cells were pelleted and resuspended in culture medium supplemented with penicillin G (1,000 U/mL), streptomycin (100 μg/mL), amphotericin B (0.25 μg/mL), 0.1% FCS, and an equal volume of rat tail collagen type I (BD Bioscience). The cellular/rat tail collagen type I suspension was immediately plated on plates precoated with 2.5 mg/mL of rat tail collagen type I. In stimulation experiments media was supplemented with recombinant EGF (final concentration of 25 ng/mL) and recombinant TGFα (final concentration of 50 ng/mL). For quantification, acinar explants were seeded in triplicate. Cell clusters were counted from at least three optical fields/well and reported as a percentage of acinar clusters and duct-like spheres. The quantification was performed in two independent experiments.

For immunofluorescent labeling of explanted pancreatic tissue, collagen gels containing pancreas organoids were fixed in 4:1 methanol/DMSO overnight at 4 °C, then washed in PBS. Collagen embedded cells were permeabilized with Triton X-100 0.1% for 5 min at room temperature and blocked with 5% normal goat serum in PBST (PBS + 0.5% Triton X-100) for 2 h at room temperature followed by sequential incubation with the primary antibodies against AMYLASE (goat polyclonal, C-20, 1:200, Santa Cruz Biotech) and CYTOKERATIN19 (rat monoclonal, TROMA-III; 1:200, DSHB-University of Iowa) and anti-goat Alexa 488 and anti-rat Alexa 594 secondary antibodies (1:200; Invitrogen) diluted in PBST, overnight at 4 °C. Following each antibody, gels were washed in PBST and counterstained with Hoechst 33342 (1 μg/mL; Invitrogen). Images were captured using Zeiss inverse fluorescent microscope.

ATAC-seq Preparation, Processing, and Analysis. The pancreata from $KC;Trp53^{+/+}$ (n = 3) and $KC;Trp53^{fl/fl}$ (n = 4) mice at ~3 and 1 mo of age, respectively, were dissociated as previously described (28), and acinar cells were sorted using a surface marker for acinar cell identity (CD49F), as well as markers to exclude ductal-like cells (CD133), erythroid (TER-119), and leukocyte cells (CD45). ATAC-seq libraries were generated from cell pellets as previously described (55). Briefly, 50,000 acinar cells from single cell suspensions were washed in PBS and resuspended in lysis buffer (10 mM Tris-HCl, pH 7.5, 10 mM NaCl, 3 mM MgCl2, an 0.1% IGEPAL CA-630), followed by centrifugation and removal of supernatant. Transposition mix (1 × TD from Illumina and 2.5 μL of Tn5 transposase in 50 μL total) was added to the cell pellet and transposition proceeded at 37 °C for 30 min. At the end of the transposition reaction, DNA was purified with a Qiagen minElute column. To create sequencing libraries, transposed DNA was amplified and indexed with Illumina Nextera sequencing primers as previously described (55). Libraries were quantified by qPCR against PhiX standard (Illumina) and each sample had technical replicates processed separately from the same single-cell suspension. Libraries were sequenced on an Illumina Hiseq (Elim Biosciences).

FASTQ files were aligned to the mouse genome mm10 using bowtie (56). Alignments were processed to remove reads that did not align to the genome or aligned to the mitochondrial genome or sex chromosomes. PCR duplicates were removed using picard tools (57). Accessible regions of the genome were called using MACS2 (58). ChrAccR (version 0.9.18) (59) was used to process aligned and filtered reads from BAM files and to summarize counts for genomic regions of interest.

To assess differential accessibility, DESeq2 was applied (60) using a model to account for mouse model, cell type, and batch. Peaks with significant changes in accessibility between p53-proficient and deficient acinar cells were further analyzed for motif enrichment using the program HOMER (61). LOLA (62) was used to compute enrichment of regions annotated in the CODEX database (63) in differentially accessible 1 kb tiling regions that exhibited lower accessibility in p53-deficient acinar cells than in p53-proficient acinar cells. Data sets for RBPJL and PTF1A ChIP-seq (GSE47459) from the CODEX database were used to plot tracks together with differentially accessible ATAC-seq peaks generated in this work.

Data, Materials, and Software Availability. ATAC-seq data have been deposited in the Gene Expression Omnibus (GEO) database (accession no. GSE224744) (64). All study data are included in the article and/or *SI Appendix*.

ACKNOWLEDGMENTS. We thank Julien Sage for critical reading of this manuscript and Patrick Neuhoefer for valuable input. This work was supported by NIH, through R21 CA169673, R01 CA140875, and R35 CA197591 grants to L.D.A.

Author affiliations: [a]Department of Radiation Oncology, Stanford University School of Medicine, Stanford, CA 94305; [b]Department of Biomedical Genetics, University of Rochester Medical Center, Rochester, NY 14642; [c]Department of Experimental Radiation Oncology, The University of Texas MD Anderson Cancer Center, Houston, TX 77030; [d]Department of Developmental Biology, Stanford University School of Medicine, Stanford, CA 94305; [e]Calico Life Sciences LLC, South San Francisco, CA 94080; [f]Department of Genetics, Stanford University School of Medicine, Stanford, CA 94305; [g]Integrative Cellular Biology and Bioinformatics, Saarland University, 66123 Saarbrücken, Germany; and [h]Department of Pathology, The Sol Goldman Pancreatic Cancer Research Center, The Johns Hopkins University School of Medicine, Baltimore, MD 21287

1. W. Park, A. Chawla, E. M. O'Reilly, Pancreatic cancer: A review. *JAMA* **326**, 851–862 (2021).
2. A. F. Hezel, A. C. Kimmelman, B. Z. Stanger, N. Bardeesy, R. A. Depinho, Genetics and biology of pancreatic ductal adenocarcinoma. *Genes Dev.* **20**, 1218–1249 (2006).
3. H. Ying *et al.*, Genetics and biology of pancreatic ductal adenocarcinoma. *Genes Dev.* **30**, 355–385 (2016).
4. A. M. Waters, C. J. Der, KRAS: The critical driver and therapeutic target for pancreatic cancer. *Cold Spring Harb. Perspect. Med.* **8**, a031435 (2018).
5. N. Bardeesy, R. A. DePinho, Pancreatic cancer biology and genetics. *Nat. Rev. Cancer* **2**, 897–909 (2002).
6. S. R. Hingorani *et al.*, Preinvasive and invasive ductal pancreatic cancer and its early detection in the mouse. *Cancer cell* **4**, 437–450 (2003).
7. R. M. M. Ferreira *et al.*, Duct- and acinar-derived pancreatic ductal adenocarcinomas show distinct tumor progression and marker expression. *Cell Rep.* **21**, 966–978 (2017).
8. C. Guerra *et al.*, Chronic pancreatitis is essential for induction of pancreatic ductal adenocarcinoma by K-ras oncogenes in adult mice. *Cancer Cell* **11**, 291–302 (2007).
9. L. C. Murtaugh, S. D. Leach, A case of mistaken identity? Nonductal origins of pancreatic "ductal" cancers. *Cancer Cell* **11**, 211–213 (2007).
10. J. P. Morris IV, D. A. Cano, S. Sekine, S. C. Wang, M. Hebrok, Beta-catenin blocks Kras-dependent reprogramming of acini into pancreatic cancer precursor lesions in mice. *J. Clin. Invest.* **120**, 508–520 (2010).
11. J. L. Kopp *et al.*, Identification of Sox9-dependent acinar-to-ductal reprogramming as the principal mechanism for initiation of pancreatic ductal adenocarcinoma. *Cancer Cell* **22**, 737–750 (2012).
12. B. M. Flowers *et al.*, Cell of origin influences pancreatic cancer subtype. *Cancer Discov.* **11**, 660–677 (2021).
13. P. Neuhöfer *et al.*, Acinar cell clonal expansion in pancreas homeostasis and carcinogenesis. *Nature* **597**, 715–719 (2021).
14. C. Guerra *et al.*, Pancreatitis-induced inflammation contributes to pancreatic cancer by inhibiting oncogene-induced senescence. *Cancer Cell* **19**, 728–739 (2011).
15. M. Kanda *et al.*, Presence of somatic mutations in most early-stage pancreatic intraepithelial neoplasia. *Gastroenterology* **142**, 730–733.e739 (2012).
16. E. Del Poggetto *et al.*, Epithelial memory of inflammation limits tissue damage while promoting pancreatic tumorigenesis. *Science* **373**, eabj0486 (2021).
17. B. J. Raphael *et al.*, Integrated genomic characterization of pancreatic ductal adenocarcinoma. *Cancer Cell* **32**, 185–203.e113 (2017).
18. W. Hosoda *et al.*, Genetic analyses of isolated high-grade pancreatic intraepithelial neoplasia (HG-PanIN) reveal paucity of alterations in TP53 and SMAD4. *J. Pathol.* **242**, 16–23 (2017).
19. J. Lüttges *et al.*, Allelic loss is often the first hit in the biallelic inactivation of the p53 and DPC4 genes during pancreatic carcinogenesis. *Am. J. Pathol.* **158**, 1677–1683 (2001).
20. S. R. Hingorani *et al.*, Trp53R172H and KrasG12D cooperate to promote chromosomal instability and widely metastatic pancreatic ductal adenocarcinoma in mice. *Cancer Cell* **7**, 469–483 (2005).
21. M. Baumgart *et al.*, Genomic instability at both the base pair level and the chromosomal level is detectable in earliest PanIN lesions in tissues of chronic pancreatitis. *Pancreas* **39**, 1093–1103 (2010).
22. E. Heinmoller *et al.*, Molecular analysis of microdissected tumors and preneoplastic intraductal lesions in pancreatic carcinoma. *Am. J. Pathol.* **157**, 83–92 (2000).
23. S. Gansauge *et al.*, Genetic alterations in chronic pancreatitis: Evidence for early occurrence of p53 but not K-ras mutations. *Br. J. Surg.* **85**, 337–340 (1998).
24. Cancer Genome Atlas Research Network, Integrated genomic characterization of pancreatic ductal adenocarcinoma. *Cancer Cell* **32**, 185–203.e113 (2017).
25. A. Maitra *et al.*, Multicomponent analysis of the pancreatic adenocarcinoma progression model using a pancreatic intraepithelial neoplasia tissue microarray. *Mod. Pathol.* **16**, 902–912 (2003).
26. K. T. Bieging, S. S. Mello, L. D. Attardi, Unravelling mechanisms of p53-mediated tumour suppression. *Nat. Rev. Cancer* **14**, 359–370 (2014).
27. C. A. Brady *et al.*, Distinct p53 transcriptional programs dictate acute DNA-damage responses and tumor suppression. *Cell* **145**, 571–583 (2011).
28. S. S. Mello *et al.*, A p53 super-tumor suppressor reveals a tumor suppressive p53-Ptpn14-yap axis in pancreatic cancer. *Cancer Cell* **32**, 460–473.e466 (2017).
29. L. J. Valente *et al.*, p53 efficiently suppresses tumor development in the complete absence of its cell-cycle inhibitory and proapoptotic effectors p21, Puma, and Noxa. *Cell Rep.* **3**, 1339–1345 (2013).
30. T. Li *et al.*, Tumor suppression in the absence of p53-mediated cell-cycle arrest, apoptosis, and senescence. *Cell* **149**, 1269–1283 (2012).
31. L. J. Valente *et al.*, p53 deficiency triggers dysregulation of diverse cellular processes in physiological oxygen. *J. Cell Biol.* **219**, e201908212 (2020).
32. P. K. Mazur *et al.*, Combined inhibition of BET family proteins and histone deacetylases as a potential epigenetics-based therapy for pancreatic ductal adenocarcinoma. *Nat. Med.* **21**, 1163–1171 (2015).
33. M. Erkan *et al.*, StellaTUM: Current consensus and discussion on pancreatic stellate cell research. *Gut* **61**, 172–178 (2012).
34. M. A. Collins *et al.*, Oncogenic Kras is required for both the initiation and maintenance of pancreatic cancer in mice. *J. Clin. Invest.* **122**, 639–653 (2012).
35. T. Baslan *et al.*, Ordered and deterministic cancer genome evolution after p53 loss. *Nature* **608**, 795–802 (2022).
36. H. Hong *et al.*, Suppression of induced pluripotent stem cell generation by the p53–p21 pathway. *Nature* **460**, 1132–1135 (2009).
37. R. M. Marion *et al.*, A p53-mediated DNA damage response limits reprogramming to ensure iPS cell genomic integrity. *Nature* **460**, 1149–1153 (2009).
38. T. Kawamura *et al.*, Linking the p53 tumour suppressor pathway to somatic cell reprogramming. *Nature* **460**, 1140–1144 (2009).
39. D. F. Tschaharganeh *et al.*, p53-dependent nestin regulation links tumor suppression to cellular plasticity in liver cancer. *Cell* **158**, 579–592 (2014).
40. J. P. Morris IV *et al.*, α-Ketoglutarate links p53 to cell fate during tumour suppression. *Nature* **573**, 595–599 (2019).
41. J. P. Morton *et al.*, Mutant p53 drives metastasis and overcomes growth arrest/senescence in pancreatic cancer. *Proc. Natl. Acad. Sci. U.S.A.* **107**, 246–251 (2010).
42. S. J. Murphy *et al.*, Genetic alterations associated with progression from pancreatic intraepithelial neoplasia to invasive pancreatic tumor. *Gastroenterology* **145**, 1098–1109.e1091 (2013).
43. D. M. Feldser *et al.*, Stage-specific sensitivity to p53 restoration during lung cancer progression. *Nature* **468**, 572–575 (2010).
44. M. Cicchini *et al.*, Context-dependent effects of amplified MAPK signaling during lung adenocarcinoma initiation and progression. *Cell Rep.* **18**, 1958–1969 (2017).
45. D. Lessel *et al.*, Dysfunction of the MDM2/p53 axis is linked to premature aging. *J. Clin. Invest.* **127**, 3598–3608 (2017).
46. D. Wu, C. Prives, Relevance of the p53-MDM2 axis to aging. *Cell Death Differ.* **25**, 169–179 (2018).
47. J. L. Van Nostrand, L. D. Attardi, Guilty as CHARGED: p53's expanding role in disease. *Cell Cycle* **13**, 3798–3807 (2014).
48. M. E. Bowen, L. D. Attardi, The role of p53 in developmental syndromes. *J. Mol. Cell Biol.* **11**, 200–211 (2019).
49. D. Nguyen, W. Liao, S. X. Zeng, H. Lu, Reviving the guardian of the genome: Small molecule activators of p53. *Pharmacol. Ther.* **178**, 92–108 (2017).
50. S. Marino, M. Vooijs, H. van Der Gulden, J. Jonkers, A. Berns, Induction of medulloblastomas in p53-null mutant mice by somatic inactivation of Rb in the external granular layer cells of the cerebellum. *Genes Dev.* **14**, 994–1004 (2000).
51. E. L. Jackson *et al.*, Analysis of lung tumor initiation and progression using conditional expression of oncogenic K-ras. *Genes Dev.* **15**, 3243–3248 (2001).
52. J. N. Jensen *et al.*, Recapitulation of elements of embryonic development in adult mouse pancreatic regeneration. *Gastroenterology* **128**, 728–741 (2005).
53. A. L. Means *et al.*, Pancreatic epithelial plasticity mediated by acinar cell transdifferentiation and generation of nestin-positive intermediates. *Development* **132**, 3767–3776 (2005), https://doi.org/10.1242/dev.01925.
54. P. K. Mazur *et al.*, SMYD3 links lysine methylation of MAP3K2 to Ras-driven cancer. *Nature* **510**, 283–287 (2014), https://doi.org/10.1038/nature13320.
55. J. D. Buenrostro, P. G. Giresi, L. C. Zaba, H. Y. Chang, W. J. Greenleaf, Transposition of native chromatin for fast and sensitive epigenomic profiling of open chromatin, DNA-binding proteins and nucleosome position. *Nat. Meth.* **10**, 1213–1218 (2013).
56. B. Langmead, S. L. Salzberg, Fast gapped-read alignment with Bowtie 2. *Nat. Meth.* **9**, 357–359 (2012).
57. Broad_Institute, Picard toolkit (Broad Institute, GitHub repository, 2019). https://broadinstitute.github.io/picard/. Accessed 15 August 2022.
58. J. M. Gaspar, Improved peak-calling with MACS2 (2018). *bioRxiv [Preprint]*. https://doi.org/10.1101/496521 (Accessed 15 August 2022).
59. F. Müller, ChrAccR: Analyzing chromatin accessibility data in R (Github, 2022). https://github.com/GreenleafLab/ChrAccR. Accessed 15 August 2022.
60. M. I. Love, W. Huber, S. Anders, Moderated estimation of fold change and dispersion for RNA-seq data with DESeq2. *Genome Biol.* **15**, 550 (2014).
61. S. Heinz *et al.*, Simple combinations of lineage-determining transcription factors prime cis-regulatory elements required for macrophage and B cell identities. *Mol. Cell* **38**, 576–589 (2010).
62. N. C. Sheffield, C. Bock, LOLA: Enrichment analysis for genomic region sets and regulatory elements in R and Bioconductor. *Bioinformatics* **32**, 587–589 (2016).
63. M. Sánchez-Castillo *et al.*, CODEX: A next-generation sequencing experiment database for the haematopoietic and embryonic stem cell communities. *Nucleic Acids Res.* **43**, D1117–1123 (2015).
64. S. S. Mello, F. Müller, S. K. Denny, W. J. Greenleaf, L. D. Attardi, The role of p53 in pancreatic cancer suppression. GEO. https://www.ncbi.nlm.nih.gov/geo/query/acc.cgi?acc=GSE224744. Deposited 7 February 2023.